Role of Ni dopant on the improvement of ZnO-based reusable photocatalytic materials

Eka Nurfani[1,📧] Azka R.Firdaus[1] Dedi Triyadi[1] Aditya Rianjanu[1]

[1] *Department of Materials Engineering, Faculty of Industrial Technology, Institut Teknologi Sumatera, Terusan Ryacudu, Way Hui, Jati Agung, Lampung Selatan 35365, Indonesia*

📧 **Corresponding author**: eka.nurfani@mt.itera.ac.id

ABSTRACT

This study investigates the impact of Ni doping on the enhancement of ZnO-based reusable photocatalytic materials. Ni concentrations derived from nickel chloride hexahydrate were 0 wt% (ZN-1), 1 wt% (ZN-2), and 3 wt% (ZN-3). Field-emission scanning electron microscopy (FESEM) analysis reveals a significant morphological transformation from flower-like structures in pure ZnO to nanoridges in Ni-doped ZnO. X-ray diffraction data indicate a reduction in crystalline quality with Ni incorporation. UV-Vis spectroscopy shows an increase in the bandgap from 3.22 eV for pure ZnO (ZN-1) to 3.34 eV for Ni-doped ZnO (ZN-2 and ZN-3). Photocatalytic efficiency improves markedly, achieving 30%, 60%, and 80% degradation for ZN-1, ZN-2, and ZN-3, respectively, after 1-hour illumination. Notably, the photocatalytic performance remains robust even after five recycling cycles. These findings reveal the potential of Ni-doped ZnO as a cost-effective, reusable, and highly efficient photocatalytic material.

Keywords: *methylene blue, spray pyrolysis, reusable photocatalyst, ZnO:Ni film*
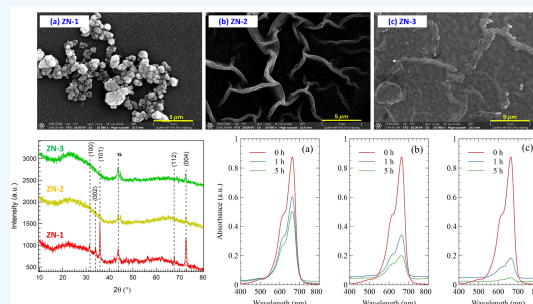
1. INTRODUCTION

The textile industry is a significant contributor to environmental pollution, particularly in water systems, due to the discharge of untreated waste containing high concentrations of organic and inorganic compounds [1]. Among these pollutants, dyes pose a serious environmental challenge as they are difficult to degrade naturally and are harmful to aquatic ecosystems. Pollution that occurs in the textile industry comes from synthetic dyes which are not environmentally friendly and are very dangerous to living creatures, which are toxic and carcinogenic [2]. Synthetic dyes have complex aromatic structures that can provide photochemical, thermal, biological, and optical stability [3]. This is what causes synthetic dyes to become an environmental problem so organic compounds need to be removed from waste before disposal [2]. One of the dyes that is often used is methylene blue [4]. Methylene Blue is an aromatic compound that is cationic heterocyclic. The concentration of methylene blue has a permissible threshold value in waters of around (5-10) mg/L [5]. Methylene Blue has the molecular formula $C_{16}H_{18}CIN_3S$ which can easily dissolve in water [4, 5], in terms of price, it is very economical and easy to obtain [3]. Methylene blue is a synthetic dye that can be used as a dye for paper, cotton, silk, and wool. In the production process, methylene blue releases some products into the environment to be used as waste which will cause dangerous effects. For example, in humans, it will have an impact on health and cause nausea, diarrheal, shortness of breath, skin irritation, and haemolysis. Thus, it is necessary to remove methylene blue from

wastewater [6].

Therefore, a waste processing technology that can accelerate the decomposition of dye waste is needed. One method that is effective, cheap, and easy to use is photodegradation. Photocatalysis is the process of chemical reactions occurring with the help of energy from photons. Here, the photon energy must be greater than the band gap of the semiconductor to generate electrons and holes [7]. There are important things about a photocatalyst system, namely the desired band gap, stability, appropriate morphology, and high surface area [8]. Many semiconductors have been employed as photocatalytic materials, such as TiO_2 [9], ZnO [10, 11], Fe_2O_3 [12], CdS [13], Nb_2O_5 [14], and CeO_2 [15]. ZnO is the material most widely used in the photocatalyst process due to its direct band gap of 3.37 eV and high exciton binding energy of 60 MeV. ZnO is also an inorganic semiconductor material that does not have toxic properties and can provide high mobility and good thermal stability.

Nanostructured ZnO can be obtained by various synthesis methods including hydrothermal [16], spray pyrolysis [11], precipitation [17], sol-gel [18], and sputtering [19]. Spray pyrolysis is a particle synthesis method that has been studied intensively because of several advantages, such as simplicity, low cost, and faster deposition time [20]. Several efforts have been made to modify the performance of ZnO-based photocatalysts via doping [21], annealing [22], heterojunction [23], and making a composite [24, 25]. Doping is a simple way to improve the optical and electrical properties of ZnO. Several dopant atoms have been successfully applied to the ZnO crystal system, such as Ti [26, 27], Sn [28], Cu [29], Fe [30], Ni
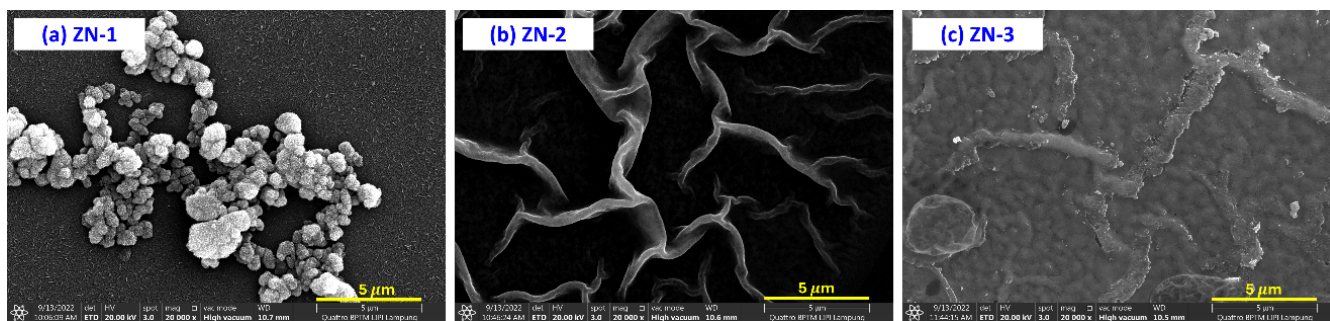
Figure 1. Morphological FESEM images of Ni-doped ZnO film on glass substrates fabricated by spray pyrolisis for (a) ZN-1, (b) ZN-2, and (c) ZN-3 samples

[31], and Al [32]. However, the application of Ni-doped ZnO film for reusable photocatalytic materials is rarely studied. In this paper, the nanostructured films were deposited using the spray pyrolysis method with various Ni concentrations. The best sample in degradation efficiency is then tested to analyze the reusable capability.

2. EXPERIMENT DETAILS

The glass substrate with dimensions of 1x1 cm was washed using acetone, ethanol, and distilled water for 10 minutes (each solution) to remove organic contaminants. At the same time, spray solutions were also prepared. Zinc Acetate Dehydrate (ZAD) and Nickel Chloride Hexahydrate (NCH) precursors were used as the source of Zn (host materials) and Ni (doping). The precursor used is ZAD because it has the highest photocatalysis effectiveness with a hexagonal structure and can produce ZnO particles with a high level of purity [32]. The precursor was dissolved in 40 mL of distilled water. To vary the concentration of Ni doping, the mass ratio between ZAD and (NCH) was weighed as presented in Table 1. The estimation of the weight percent of NCH is 0% (ZN-1 sample), 1% (ZN-2 sample), and 3% (ZN-3 sample). After that, the solution was stirred for 60 minutes at 800 rpm at room temperature until it became homogeneous. The homogeneous solution was placed into the spray tank. The commercial spray machine used in this study was an air compressor nebulizer (Elvasense NEB39). The distance between the nozzle and substrate was kept at around 2 cm. The spray rate was 0.19-0.40 mL/min with a 4.01-4.48 μm particle size. Before the spray pyrolysis, the substrate is first heated on a hotplate at 400°C for 10 minutes. This aims to distribute the temperature evenly over the entire surface during the spray process. Deposition time was 15 mins at 400°C.

Furthermore, field-emission scanning electron microscopy (FESEM) was employed to determine the morphology of the film deposited by the spray pyrolysis method. X-ray diffraction (XRD) technique was used to determine the crystallinity of the samples. Ultraviolet-Visible (UV-Vis) spectroscopy was used to determine the optical bandgap of the sample and photocatalytic performance. The photocatalytic activity was analyzed using methylene blue or MB ($C_{16}H_{18}ClN_3S$) with a concentration of 10 ppm as the pollutant sample. The film was soaked in MB solution. It was then exposed to a 50 W halogen lamp for 0, 1, and 5 hours. The distance between the sample and the halogen lamp is 12 cm. After being exposed to the specified time, the degradation results of methylene blue were measured using UV-Vis spectroscopy. To check the reusable photocatalytic performance, the film was immersed
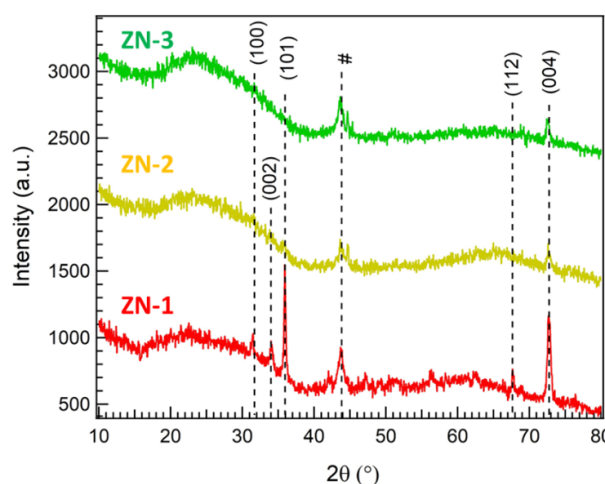
Figure 2. XRD pattern of the ZN-1, ZN-2, and ZN-3 samples

in alcohol before the subsequent photocatalytic measurement was performed. This measurement was repeated for 5 cycles.

Table 1. The ratio of precursor mass (ZAD and NCH) for fabricating Ni-doped ZnO film with various Ni concentrations.

Samples	DI water (mL)	ZAD (gr)	NCH (gr)
ZN-1	40	4.3900	0
ZN-2	40	4.3461	0.0439
ZN-3	40	4.1710	0.1317

3. RESULTS AND DISCUSSION

3.1 Surface Morphology

Morphological of the film deposited by the spray pyrolysis was then characterized using the FESEM technique, as shown in Figure 1. The surface morphology of the pure ZnO film (ZN-1) is nanorice in the background. At the surface, the particles agglomerate into a flower-like structure with an estimated diameter of around 1.3 μm by sampling 50 points. For the Ni-doped ZnO films (ZN-2 and ZN-3 samples), the morphology changes significantly into nanoridges, while the presence of a flower-like structure cannot be found. Ni doping changes the surface energy of ZnO, which affects the aggregation and growth of particles [33]. Ni dopant may reduce the surface energy of non-polar faces of ZnO. This condition enables the nanostructures to grow in the lateral direction and influences how particles agglomerate and grow,
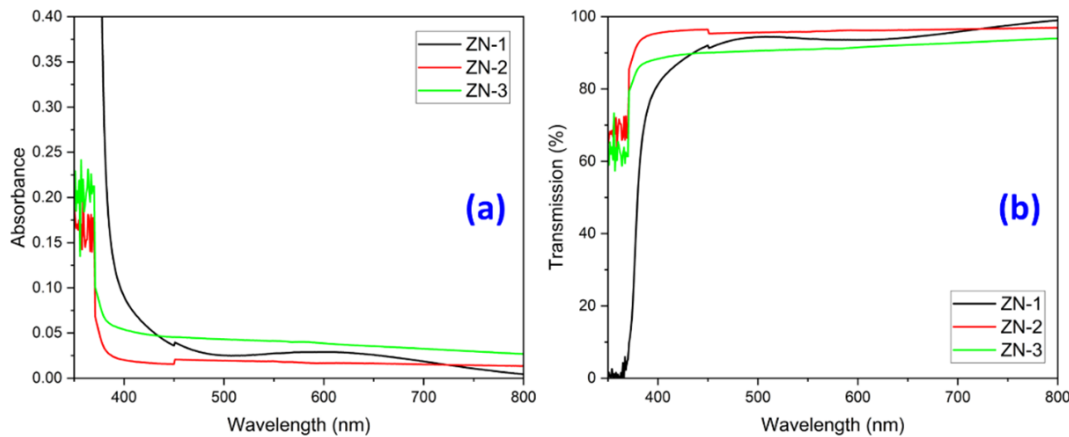
Figure 3. (a) UV-Vis absorption and (b) transmission spectra of Ni-doped ZnO films for various Ni precursor concentrations of 0% (ZN-1), 1% (ZN-2), and 3% (ZN-3)

shifting from flower-like structures to nanoridges [33]. In the ZN-2 sample, the nanoridges structure is observed, while the background structure cannot be observed due to the significant height of the hill. In the ZN-3 sample, the background structure is observed, from nanorice to nanoparticle structure, due to agglomeration. The average particle size of the ZN-3 sample is 1̄.5 μm.
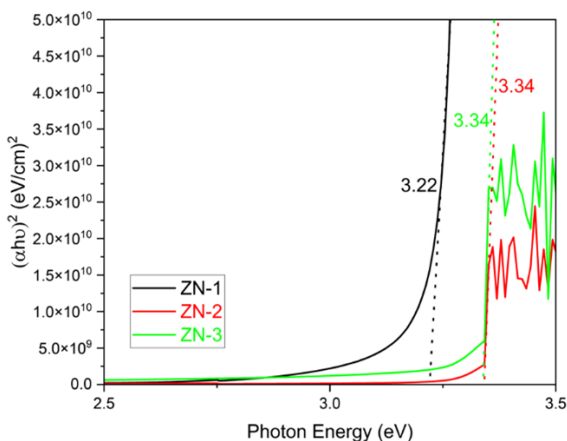
Figure 4. Tauc-plot method to calculate the optical bandgap of ZN1, ZN2, and ZN3 samples

3.2 Structural Properties

Figure 2 shows the diffraction patterns of ZN-1, ZN-2, and ZN-3 samples at 2θ of 10-80°. XRD is important to determine the crystal structure, lattice parameters, and possibility of other phase formations in the film. In the ZN-1 samples, crystalline planes of (100), (002), (101), (112), and (004) are observed at 2θ of 31.50°, 34.11°, 35.91°, 67.64°, and 72.61° respectively. It indicates the formation of hexagonal wurtzite structures (JCPDS no. 89-1397). No peaks contributed from Ni, NiO, or ZnNiO are observed, indicating the success of the inserting of Ni dopant into the ZnO host. In the ZN-2 and ZN-3 samples, the intensity of these planes is reduced significantly, indicating crystal deterioration after inserting the Ni dopant. The Ni^{2+} ion (0.69 Å) substitutes the Zn^{2+} sites (0.74 Å) in the ZnO lattice, causing lattice mismatch and inducing strain [33]. This strain disrupts the regular periodic

arrangement of atoms, reducing the crystallinity and leading to broader and less intense diffraction peaks.

3.3 Optical Properties

UV-Vis Spectrophotometer was employed to determine the optical properties of the samples (Figure 3). Absorbance spectra showed that the highest intensity was obtained in ZN-1 samples in the UV region (300–400 nm). By introducing Ni doping, both ZN-2 and ZN-3 show significantly reduced absorbance intensities. Ni doping can introduce defects or distortions into the ZnO lattice. This disruption may reduce the crystallinity or introduce non-radiative recombination centers, leading to lower optical absorption. On the other hand, the transmission spectra reveal that ZN-1 has the lowest transmission, while ZN-2 and ZN-3 exhibit higher transmission across the UV-Vis region. Higher transmission in Ni-doped samples suggests a decrease in light interaction within the film, possibly due to reduced optical density due to structural defects caused by Ni doping.

Furthermore, the band gap energy of ZN-1, ZN-2, and ZN-3 thin films was obtained by plotting the absorption data using the direct transition equation. The $(\alpha h\nu)^2$ vs ($h\nu$) plot, known as the Tauc-plot method [34], is shown in Figure 4. Linear extrapolation of the curve to the zero-absorption line gives the energy band gap for the direct transition. The band gap energy values produced in the samples of ZN-1, ZN-2, and ZN-3 are 3.22 eV, 3.34 eV, and 3.34 eV. A smaller band gap means that electron-hole pairs are easily formed, which directly facilitates the photocatalysis process.

3.4 Photocatalytic Performance

Photocatalytic tests were carried out for 0, 1, and 5 hours in 10 ppm methylene blue solution, as shown in Figure 5. The testing was carried out using a UV-Vis spectrophotometer to determine the change in the absorption spectrum, which directly correlates to the concentration of methylene blue. The decrease in methylene blue concentration is indicated by the decrease in the absorbance spectrum. Photocatalytic activity of the ZN-1, ZN-2, and ZN-3 samples is observed by increasing the illumination time. It is indicated by the reduction of the absorbance intensity for 1 and 5 h illumination. It has resulted from an electron excitation from the valence band to the conduction band. Electrons in the conduction band interact with oxygen so that they help in the
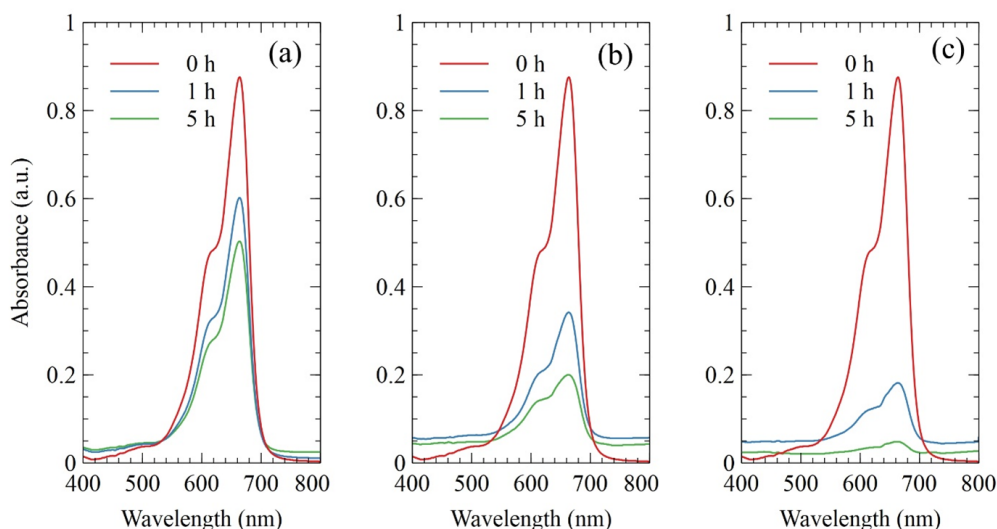
Figure 5. UV-Vis absorption spectra of 10 ppm methylene blue that was degraded by (a) ZN-1, (b) ZN-2, and (c) ZN-3 with different irradiation times.
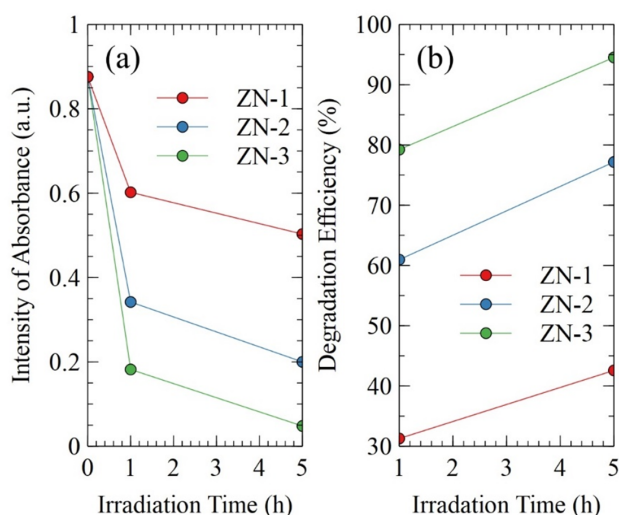
Figure 6. (a) Absorbance intensity and (b) degradation efficiency of methylene blue by immersing ZnO-based photocatalytic materials for various irradiation times and Ni concentrations.

electron transfer process to produce superoxide radical ions $\cdot O_2^-$, while methylene blue molecules will bind to holes in the valence band on the surface of the photocatalyst and produce hydroxyl radicals $\cdot OH$. This reaction aims to act as a strong oxidizer in the process of oxidizing organic compounds, such as methylene blue. Increasing the illumination time causes an increase in degradation. This is caused by the increasing number of photons hitting ZnO, thereby increasing the formation of hydroxyl radicals as a pollutant oxidizer.

Figure 6(a) shows the intensity of the main absorbance peak for all samples. In general, the increase in the irradiation time decreases the absorbance intensity. The ZN-3 sample shows the lowest absorbance intensity for 1 and 5 hours of irradiation times. This condition leads to the best degradation efficiency obtained from the ZN-3 sample, as shown in Figure

6(b). The degradation efficiency is calculated by

$$efficiency(\%) = \left(\frac{I_0 - I}{I_0}\right) \times 100\% \qquad (1)$$

where I_0 is the initial intensity (before photocatalysis) and I is the final intensity. The degradation efficiency of 1 hour illumination time is 30% (ZN-1), 60% (ZN-2), and 80% (ZN-3). By increasing the illumination time up to 5 hours, the degradation efficiency is 43% (ZN-1), 76% (ZN-2), and 95% (ZN-3). Although the overall bandgap may slightly increase, Ni doping often introduces mid-gap states or d-d transitions related to Ni ions. These states allow ZnO to absorb a wider spectrum of light, particularly into the visible range. This increased absorption contributes to more effective utilization of the incident light for ROS (reactive oxygen species) generation such as hydroxyl radicals and superoxide anions.

Figure 7 shows the C/C_0 and $\ln C/C_0$ for various irradiation and doping concentrations. The C/C_0 data shows how the pollutant concentration changes over time during photocatalysis. This value decreases by increasing degradation time. The plot of $\ln C/C_0$ provides a more quantitative understanding of the reaction mechanism. It determines the reaction kinetics, especially if the process follows pseudo-first-order kinetics. A fitting of the straight line indicates pseudo-first-order reaction kinetics. The slope (m) of the line corresponds to the reaction rate constant (k) as expressed in the following equation

$$\ln\left(\frac{C}{C_0}\right) = -kt \qquad (2)$$

the obtained rate constants are 0.04 (ZN-1), 0.13 (ZN-2), and 0.33 (ZN-3). A larger k value for the ZN-3 sample indicates faster degradation and better photocatalytic efficiency.

ZnO films prepared via spray pyrolysis are considered excellent candidates for photocatalytic applications, especially for recycling purposes. Figure 8 is the reusable test for the ZN-3 sample for 5-hour irradiation times. The degradation efficiency is 95% (cycle 1), 85% (cycle 2), 72% (cycle 3), 82% (cycle 4), and 82% (cycle 5). The lowest degradation efficiency
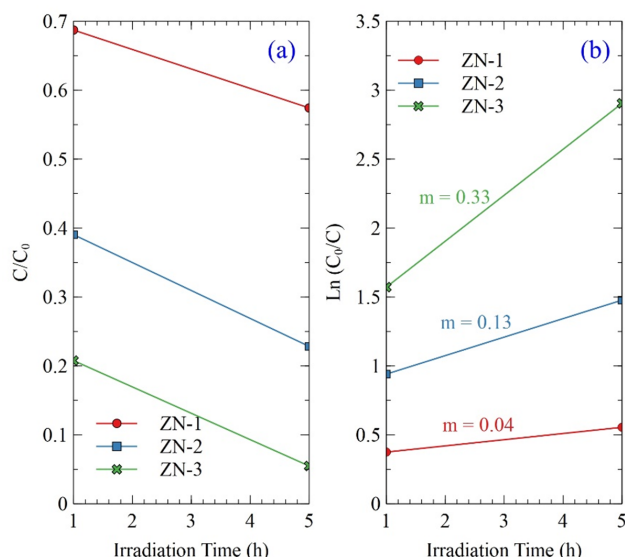
Figure 7. (a) Concentration of methylene blue and (b) degradation rate as the function of irradiation time by using ZnO-based photocatalytic materials

in cycle 3 may be caused by the cleaning process that only used distilled water rinse. Films deposited via spray pyrolysis adhere well to substrates, ensuring long-term stability during cyclic use. ZnO in the form of a thin film is easy to handle and recover after the reaction. Unlike powders, it does not require filtration or centrifugation, making recycling straightforward. This technique is low-cost, scalable, and allows for uniform deposition over large areas, making it suitable for industrial-scale applications.
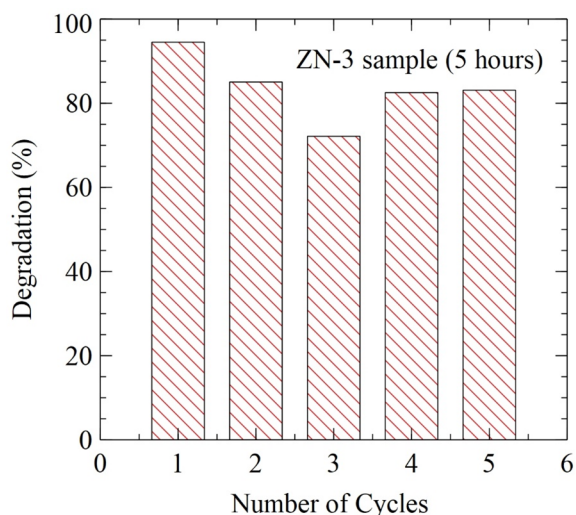
Figure 8. Performance of reusable photocatalytic materials by using ZN-3 sample for 5 cycles with an irradiation time of 5 h

4. CONCLUSION

This study demonstrates that Ni doping significantly enhances the photocatalytic performance and reusability of ZnO-based materials. The incorporation of Ni induces a

morphological transformation from flower-like structures to nanoridges and reduces crystalline quality, as observed in FESEM and XRD analyses. Despite a slight increase in the bandgap from 3.22 eV to 3.34 eV, the photocatalytic efficiency improves substantially, achieving up to 80% degradation after 1-hour illumination. Furthermore, the materials exhibit excellent stability, maintaining high photocatalytic efficiency even after five recycling cycles. These results highlight the potential of Ni-doped ZnO as a low-cost, reusable, and effective photocatalytic material for environmental applications, paving the way for sustainable water and air purification technologies.

CONFLICT OF INTEREST

The authors declare that there are no conflicts of interest.

DATA AVAILABILITY

The datasets generated and analyzed during the current study are available from the corresponding author upon reasonable request.

REFERENCES

[1] R. Gayatri, T. Agustina, R. Moeksin, D. Bahrin, G. Gustini, Preparation and Characterization of ZnO-Zeolite Nanocomposite for Photocatalytic Degradation by Ultraviolet Light, Journal of Ecological Engineering 22 (2) (2021) 178–186. https://doi.org/10.12911/22998993/131031.

[2] K. M. Lee, C. W. Lai, K. S. Ngai, J. C. Juan, Recent developments of zinc oxide based photocatalyst in water treatment technology: A review, Water Research 88 (2016) 428–448. https://doi.org/10.1016/j.watres.2015.09.045.

[3] J.-Z. Guo, B. Li, L. Liu, K. Lv, Removal of methylene blue from aqueous solutions by chemically modified bamboo, Chemosphere 111 (2014) 225–231. https://doi.org/10.1016/j.chemosphere.2014.03.118.

[4] M. Fayazi, M. A. Taher, D. Afzali, A. Mostafavi, Enhanced Fenton-like degradation of methylene blue by magnetically activated carbon/hydrogen peroxide with hydroxylamine as Fenton enhancer, Journal of Molecular Liquids 216 (2016) 781–787. https://doi.org/10.1016/j.molliq.2016.01.093.

[5] H.-P. Jing, C.-C. Wang, Y.-W. Zhang, P. Wang, R. Li, Photocatalytic degradation of methylene blue in ZIF-8, RSC Adv. 4 (97) (2014) 54454–54462. https://doi.org/10.1039/C4RA08820D.

[6] M. Khodaie, N. Ghasemi, B. Moradi, M. Rahimi, Removal of Methylene Blue from Wastewater by Adsorption onto $ZnCl_2$ Activated Corn Husk Carbon Equilibrium Studies, Journal of Chemistry 2013 (1) (2013) 383985. https://doi.org/10.1155/2013/383985.

[7] A. Abdul Mutalib, N. Jaafar, ZnO photocatalysts applications in abating the organic pollutant contamination: A mini review, Total Environment Research Themes 3-4 (2022) 100013. https://doi.org/10.1016/j.totert.2022.100013.

[8] N. Roy, S. Chakraborty, ZnO as photocatalyst: An approach to waste water treatment, Materials Today: Proceedings 46 (2021) 6399–6403. https://doi.org/10.1016/j.matpr.2020.06.264.

[9] S. Horikoshi, N. Serpone, Can the photocatalyst TiO2 be incorporated into a wastewater treatment method? Background and prospects, Catalysis Today 340 (2020) 334–346. https://doi.org/10.1016/j.cattod.2018.10.020.

[10] M. P. Ali, A. Rianjanu, N. Pertiwi, R. Kurniawan, R. Marlina, E. Nurfani, Optical and photocatalytic properties of ZnO:Mg film grown by spray pyrolysis, Journal of the Iranian Chemical Society 21 (10) (2024) 2733–2741. https://doi.org/10.1007/s13738-024-03105-8.

[11] E. Nurfani, M. P. Ali, A. Rianjanu, L. Nulhakim, M. S. Anrokhi, G. T. Kadja, Effect of solution molarity on the optical and photo-

catalytic properties of sprayed ZnO film, Materials Chemistry and Physics 309 (2023) 128412. https://doi.org/10.1016/j.matchemphys.2023.128412.

[12] C. Hitam, A. Jalil, A review on exploration of Fe2O3 photocatalyst towards degradation of dyes and organic contaminants, Journal of Environmental Management 258 (2020) 110050. https://doi.org/10.1016/j.jenvman.2019.110050.

[13] L. Cheng, Q. Xiang, Y. Liao, H. Zhang, CdS-Based photocatalysts, Energy & Environmental Science 11 (6) (2018) 1362–1391. https://doi.org/10.1039/C7EE03640J.

[14] T. Taher, Z. Yu, E. K. A. Melati, A. Munandar, R. Aflaha, K. Triyana, Y. G. Wibowo, K. Khairurrijal, A. Lesbani, A. Rianjanu, Enabling dual-functionality material for effective anionic and cationic dye removal by using Nb2O5/MgAl-LDH nanocomposites, Journal of Hazardous Materials Letters 5 (2024) 100103. https://doi.org/10.1016/j.hazl.2024.100103.

[15] A. Rianjanu, K. D. P. Marpaung, C. Siburian, S. A. Muhtar, N. I. Khamidy, J. Widakdo, N. Yulianto, R. Aflaha, K. Triyana, T. Taher, Enhancement of photocatalytic activity of CeO2 nanorods through lanthanum doping (La–CeO2) for the degradation of Congo red dyes, Results in Engineering 23 (2024) 102748. https://doi.org/10.1016/j.rineng.2024.102748.

[16] D. Oktapia, E. Nurfani, B. A. Wahjoedi, L. Nulhakim, G. T. M. Kadja, Seedless hydrothermal growth of hexagonal prism ZnO for photocatalytic degradation of methylene blue: the effect of pH and post-annealing treatment, Semiconductor Science and Technology 38 (10) (2023) 105005. https://doi.org/10.1088/1361-6641/acf397.

[17] B. Bekele, A. Degefa, F. Tesgera, L. T. Jule, R. Shanmugam, L. Priyanka Dwarampudi, N. Nagaprasad, K. Ramasamy, Green versus Chemical Precipitation Methods of Preparing Zinc Oxide Nanoparticles and Investigation of Antimicrobial Properties, Journal of Nanomaterials 2021 (2021) 1–10. https://doi.org/10.1155/2021/9210817.

[18] E. I. Naik, H. B. Naik, R. Viswanath, B. Kirthan, M. Prabhakara, Effect of zirconium doping on the structural, optical, electrochemical and antibacterial properties of ZnO nanoparticles prepared by sol-gel method, Chemical Data Collections 29 (2020) 100505. https://doi.org/10.1016/j.cdc.2020.100505.

[19] M. A. K. Purbayanto, E. Nurfani, M. A. Naradipa, R. Widita, A. Rusydi, Y. Darma, Enhancement in green luminescence of ZnO nanorods grown by dc-unbalanced magnetron sputtering at room temperature, Optical Materials 108 (2020) 110418. https://doi.org/10.1016/j.optmat.2020.110418.

[20] E. Nurfani, A. Lailani, W. Kesuma, M. Anrokhi, G. Kadja, M. Rozana, UV sensitivity enhancement in Fe-doped ZnO films grown by ultrafast spray pyrolysis, Optical Materials 112 (2021) 110768. https://doi.org/10.1016/j.optmat.2020.110768.

[21] S. Iqbal, A. Bahadur, M. Javed, O. Hakami, R. M. Irfan, Z. Ahmad, A. AlObaid, M. M. Al-Anazy, H. B. Baghdadi, H. S. Abd-Rabboh, T. I. Al-Muhimeed, G. Liu, M. Nawaz, Design Ag-doped ZnO heterostructure photocatalyst with sulfurized graphitic C3N4 showing enhanced photocatalytic activity, Materials Science and Engineering: B 272 (2021) 115320. https://doi.org/10.1016/j.mseb.2021.115320.

[22] A. Suguna, S. Prabhu, M. Selvaraj, M. Geerthana, A. Silambarasan, M. Navaneethan, R. Ramesh, C. Sridevi, Annealing effect on photocatalytic activity of ZnO nanostructures for organic dye degradation, Journal of Materials Science: Materials in Electronics 33 (11) (2022) 8868–8879. https://doi.org/10.1007/s10854-021-06942-y.

[23] R. M. Mohamed, A. A. Ismail, Photocatalytic reduction and removal of mercury ions over mesoporous CuO/ZnO S-scheme heterojunction photocatalyst, Ceramics International 47 (7) (2021) 9659–9667. https://doi.org/10.1016/j.ceramint.2020.12.105.

[24] R. Qin, F. Meng, M. W. Khan, B. Yu, H. Li, Z. Fan, J. Gong, Fabrication and enhanced photocatalytic property of TiO2-ZnO composite photocatalysts, Materials Letters 240 (2019) 84–87. https://doi.org/10.1016/j.matlet.2018.12.139.

[25] Z. Fan, C. Li, M. Xu, Fabrication of ZnO/Ag photocatalyst and its photocatalytic degradation properties on trimethylamine, Journal of the Iranian Chemical Society 21 (8) (2024) 2121–2126. https://doi.org/10.1007/s13738-024-03055-1.

[26] E. Nurfani, C. D. Satrya, I. Abdurrahman, I. M. Sutjahja, T. Winata, K. Takase, A. Rusydi, Y. Darma, Weakening of excitonic screening effects in Ti Zn1-O thin films, Thin Solid Films 645 (2018) 399–404. https://doi.org/10.1016/j.tsf.2017.11.015.

[27] E. Nurfani, R. Kurniawan, T. Aono, K. Takeda, Y. Shirai, I. M. Sutjahja, A. Rusydi, T. Winata, K. Takase, Y. Darma, Defect-induced excitonic recombination in Ti $_x$ Zn$_{1\ x}$ O thin films grown by DC-unbalanced magnetron sputtering, Japanese Journal of Applied Physics 56 (11) (2017) 112101. https://doi.org/10.7567/JJAP.56.112101.

[28] E. Nurfani, M. Purbayanto, R. Akutsu, M. Naradipa, L. Diguna, M. Birowosuto, K. Takase, A. Rusydi, Y. Darma, Tuning the excitonic properties of ZnO:Sn thin films, Optical Materials 88 (2019) 111–116. https://doi.org/10.1016/j.optmat.2018.11.015.

[29] E. Nurfani, W. Kesuma, A. Lailani, M. Anrokhi, G. Kadja, M. Rozana, W. Sipahutar, M. Arif, Enhanced UV sensing of ZnO films by Cu doping, Optical Materials 114 (2021) 110973. https://doi.org/10.1016/j.optmat.2021.110973.

[30] E. Nurfani, Y. K. Lature, M. S. Anrokhi, Morphological modification and UV sensitivity enhancement in ZnO:Fe films with a seed layer, Optical Materials 122 (2021) 111658. https://doi.org/10.1016/j.optmat.2021.111658.

[31] I. Ahmad, M. Aslam, U. Jabeen, M. N. Zafar, M. N. K. Malghani, N. Alwadai, F. H. Alshammari, A. S. Almuslem, Z. Ullah, ZnO and Ni-doped ZnO photocatalysts: Synthesis, characterization and improved visible light driven photocatalytic degradation of methylene blue, Inorganica Chimica Acta 543 (2022) 121167. https://doi.org/10.1016/j.ica.2022.121167.

[32] N. Azizah, S. Muhammady, M. A. K. Purbayanto, E. Nurfani, T. Winata, E. Sustini, R. Widita, Y. Darma, Influence of Al doping on the crystal structure, optical properties, and photodetecting performance of ZnO film, Progress in Natural Science: Materials International 30 (1) (2020) 28–34. https://doi.org/10.1016/j.pnsc.2020.01.006.

[33] S. H. Zyoud, V. Ganesh, C. A. Che Abdullah, I. S. Yahia, A. H. Zyoud, A. F. I. Abdelkader, M. G. Daher, M. Nasor, M. Shahwan, H. Y. Zahran, M. S. Abd El-sadek, E. A. Kamoun, S. M. Altarifi, M. S. Abdel-wahab, Facile Synthesis of Ni-Doped ZnO Nanostructures via Laser-Assisted Chemical Bath Synthesis with High and Durable Photocatalytic Activity, Crystals 13 (7) (2023) 1087. https://doi.org/10.3390/cryst13071087.

[34] J. Tauc, Optical properties and electronic structure of amorphous Ge and Si, Materials Research Bulletin 3 (1) (1968) 37–46. https://doi.org/10.1016/0025-5408(68)90023-8.